Journal of Materials Chemistry C

Design Two-Dimensional Electron Gas via Polarization Discontinuity from Large-Scale First-Principles Calculations

Journal:	*Journal of Materials Chemistry C*
Manuscript ID	TC-ART-04-2018-001893.R1
Article Type:	Paper
Date Submitted by the Author:	24-May-2018
Complete List of Authors:	Cheng, Jianli; University of California, San Diego, Department of NanoEngineering Yang, Kesong; University of California, San Diego, NanoEngineering Department

Journal Name

ARTICLE TYPE

Cite this: DOI: 10.1039/xxxxxxxxxx

Design Two-Dimensional Electron Gas via Polarization Discontinuity from Large-Scale First-Principles Calculations†

Jianli Cheng and Kesong Yang*

Received Date
Accepted Date

DOI: 10.1039/xxxxxxxxxx

www.rsc.org/journalname

Two-dimensional electron gas (2DEG) formed at the interface between two insulating perovskite oxides has provided a versatile playground to explore emergent interfacial electronic and magnetic properties. Here we show that by using high-throughput first-principles calculations and a group of effective materials descriptors based on bulk perovskite materials, we are able to rapidly design more than 300 candidate 2DEG systems based on nonpolar/nonpolar perovskite heterostructures (HS). These HS are built from 34 nonpolar piezoelectric perovskite oxides that can show polarization behavior under epitaxial compressive strain and can be further divided into six groups of materials based on B-site elements: Ti-, Zr-, Hf-, Si-, Ge-, and Sn-based oxides. By taking one compound as the substrate from each group and building all the possible HS with an appropriate lattice mismatch $0 < f < 6\%$, we have carried out comprehensive first-principles calculations to verify the formation of 2DEG in these HS. It has been found that there indeed exist a stable polarization and interfacial 2DEG for most of the selected HS. This work demonstrates an efficient way to perform high-throughput design of perovskite-oxide-based functional materials.

1 INTRODUCTION

Artificial interfaces between two perovskite oxides provide an ideal platform to tailor material properties by manipulating interplay between electronic and lattice degrees of freedom.[1–3] In particular, recent progress in thin film growth techniques has greatly stimulated interfacial engineering of complex oxide heterostructures (HS) into a flourishing field, giving unprecedented access to emerging materials properties for enhanced functionality and device applications.[4,5] In principle, the novel material properties at oxide interfaces are a consequence of local symmetry breaking, charge transfer, electrostatic coupling, frustration, or epitaxial strain at the heterointerface.[6] For instance, two-dimensional electron gas (2DEG), quantum hall effect,[7,8] superconductivity,[9] magnetism,[10] nanoscale-controlled metal-insulator transition,[11] and spin-to-charge conversion[12] have been observed at perovskite-oxide-based interfaces. Among these emerging materials properties, the 2DEG at the interface of two wide-band-gap perovskite insulators has been an active research topic in the past decades not only from the fundamental physics perspective but also because of its potential applications in the nanoelectronics.[13–17]

According to interfacial configurations of perovskite oxide HS, there are essentially three types of interfaces that can form the 2DEG.[16] The first one is polar/nonpolar interface, such as $(LaO)^{+}/(TiO_2)^{0}$ in the $LaAlO_3/SrTiO_3$ HS. The 2DEG formation mechanism in $LaAlO_3/SrTiO_3$ is primarily attributed to the intrinsic electronic reconstruction, *i.e.*, polar catastrophe.[13,18] Here and hereafter, for convenience, by following the denomination of polar/nonpolar $(LaO)^{+}/(TiO_2)^{0}$ interface in the $LaAlO_3/SrTiO_3$ HS, we define the charged layer of a perovskite oxide along [001] direction like $(LaO)^{+}$ as polar and the neutral layer like $(TiO_2)^{0}$ as nonpolar. Accordingly, the corresponding bulk oxides are considered as polar or nonpolar. Other mechanisms, such as the oxygen vacancies,[19,20] interface cation mixing,[21] and internal structural deformation,[22,23] have also been proposed to explain the origins of the interfacial 2DEG conductivity. Despite the controversy, the polar/nonpolar interfacial configuration plays a critical role in forming the interfacial conductivity. For example, in addition to the intensively studied $LaAlO_3/SrTiO_3$ HS, other polar/nonpolar HS have also been synthesized and found to host the 2DEG as well, such as $LaTiO_3/SrTiO_3$,[24] $GdTiO_3/SrTiO_3$[25] and $NdGaO_3/SrTiO_3$.[26]

The second interfacial configuration to produce 2DEG in the perovskite oxide HS is polar/polar interface such as $(LaO)^{+1}/(TaO_2)^{+1}$ in the $LaAlO_3/KTaO_3$.[2,16,27] In the computational side, by using first-principles electronic structures calcula-

Department of NanoEngineering, University of California San Diego, 9500 Gilman Drive, Mail Code 0448, La Jolla, California 92093-0448, USA. Tel: +1-858-534-2514; E-mail: kesong@ucsd.edu

† Electronic Supplementary Information (ESI) available: [details of any supplementary information available should be included here]. See DOI: 10.1039/b000000x/

tions, we have proposed to create 2DEG in the polar/polar perovskite oxide HS based on the $LaAlO_3/A^+B^{5+}O_3$ (A = Na and K, B = Nb and Ta).[16] Its interfacial conductivity is attributed to two donor layers, *i.e.*, $(LaO)^{+1}$ and $(BO_2)^+$ (B=Nb and Ta), in this polar/polar system, which has larger interfacial charge carrier density than the polar/nonpolar $LaAlO_3/SrTiO_3$ system. In the experimental side, very recently, $LaAlO_3/KTaO_3$ interface has been successfully fabricated, and a highly mobile 2DEG has been observed at the interface;[2] Zou *et al.* has prepared a $LaTiO_3/KTaO_3$ HS and reported a 2DEG with a higher carrier mobility than the doped bulk $SrTiO_3$ at this interface.[27]

The third possible interfacial configuration of the perovskite oxide HS is nonpolar/nonpolar interface. Besides the HS relying on the polar oxide layers to create the interfacial 2DEG, very recently, the nonpolar/nonpolar oxide HS have also been found to be able to produce 2DEG via the piezoelectric polarization, such as the $CaZrO_3/SrTiO_3$, both from the experiment and first-principles electronic structure calculations.[15,28] In the $CaZrO_3/SrTiO_3$ HS, there exists an insulator-to-metal transition when the $CaZrO_3$ film thickness goes beyond 6 unit cells, and the 2DEG is attributed to the lattice-mismatch-induced polarization in the $CaZrO_3$ film.[28] Our first-principles computational study has confirmed the formation of the interfacial metallic states and shows that the compressive strain in the $CaZrO_3$ film leads to a polarization discontinuity at the interface that drives the charges from the $CaZrO_3$ film to the $SrTiO_3$ substrate.[15] Moreover, unlike polar/nonpolar and polar/polar HS, which rely on a specific interfacial termination to form the 2DEG, the creation of 2DEG in $CaZrO_3/SrTiO_3$ systems is less sensitive to the interfacial structure and can be formed at both interfacial terminations. Soon later, we further proposed several other nonpolar/nonpolar perovskite oxide HS systems based on the $AHfO_3/SrTiO_3$ (A = Ca, Sr, and Ba).[29]

Other than the Zr- and Hf-involved perovskite oxide HS, the Ti-involved HS have also been found to exhibit the discontinuous polarization across the heterointerface, such as $PbTiO_3/SrTiO_3$ and $BaTiO_3/SrTiO_3$.[30,31] It is known that many perovskite oxides are equipped with a ferroelectric or piezoelectric property (under an epitaxial strain). Therefore, considering the formation of a polarization discontinuity in the nonpolar/nonpolar oxide HS and its ability to create a robust interfacial 2DEG, we expect that there could be potentially more nonpolar/nonpolar perovskite oxide HS systems that can produce 2DEG. In this work, by employing high-throughput first-principles calculations and a group of combinatorial materials descriptors, we have successfully identified 34 nonpolar piezoelectric perovskite oxides, which can be divided into six groups of oxides, Ti-, Zr-, Hf-, Si-, Ge-, and Sn-based oxides. Based on these 34 nonpolar compounds, we are further able to construct 311 nonpolar/nonpolar HS systems that can potentially form a polarization discontinuity and a resulting 2DEG at their interface. This work has demonstrated an efficient approach to perform high-throughput design of perovskite-oxide-based functional materials.

2 Computational Details

The spin-polarized Density Functional Theory (DFT) electronic structure calculations were performed using Vienna *Ab-initio* Simulation Package (VASP),[32,33] along with the projector augmented wave potentials[34] and Perdew-Burke-Ernzerhof generalized gradient approximation (GGA).[35] All the structures were optimized by minimizing atomic forces up to 0.03 eV/Å. The cutoff energy for the plane-wave expansion was set to 450 eV and the break condition for electronic self-consistency loop was assumed for a total energy convergence of less than 10^{-6} eV. The Γ-centered *k*-point grid for Brillouin zone sampling was set to $6\times6\times6$ in the ionic relaxation and $12\times12\times12$ in the static calculation. The initial magnetic moments were set to 5 μ_B on transition metals and rare-earth elements, and 1 μ_B on all other types of ions.

The strongly constrained and appropriately normed (SCAN) meta-GGA[36] and hybrid DFT calculations within Heyd-Scuseria-Ernzerhof (HSE) formalism[37] with 20% Hartree-Fock exchange were further employed to improve the lattice parameter and band gap calculations for the screened bulk perovskite oxides. A slab model with a 20 Å vacuum layer along the [001] direction was used to model the nonpolar/nonpolar HS. The thickness of substrate was set to 5 unit cells and the thickness of film was varied from 2 to 15 unit cells to investigate the critical thickness to form the interfacial 2DEG. In the ionic relaxations of HS, all the layers of film and first two unit cells of the substrates were allowed to relax and the three remaining unit cells of the substrate were freezed to mimic the experimental epitaxial film growth process. The *k*-point grid was set to $4\times4\times1$ in the ionic relaxation and $8\times8\times1$ in the static calculation for the HS models.

3 RESULTS AND DISCUSSION

3.1 Material Descriptors of Bulk Perovskites

A successful high-throughput materials screening lies in the development of effective materials descriptors.[38] In our prior work, we have carried out a high-throughput design of 2DEG systems based on polar/nonpolar perovskite oxide HS, in which the materials descriptors of forming interfacial 2DEG include the polar/nonpolar character, lattice mismatch, band gaps, and conduction band edges of polar perovskite oxides.[17] In that work, we built a perovskite-oxide-oriented quantum materials database that contains 3885 cubic ABO_3 compounds, and successfully identified 292 semiconductors and insulators ($E_g > 0$). Here we employ the material descriptor of $E_g > 0.25$ eV as the first condition to screen the bulk piezoelectric oxides on the basis of prior results, and are able to narrow down the list of candidate bulk perovskite oxides from 292 to 262.[39] In terms of the 2DEG formation driven by the polarization discontinuity at nonpolar/nonpolar perovskite oxide interfaces, it requires that the substrate is a non-polarized oxide such as $SrTiO_3$, and the film is a ferroelectric or piezoelectric oxide such as $PbTiO_3$, $CaZrO_3$, and $CaHfO_3$.[15,29,30] Note that the piezoelectric character should be caused by the lattice-mismatch-induced compressive strain in the epitaxial growth. Therefore, besides the nonpolar character, lattice mismatch, band gaps, and band edges, the polarization character of a perovskite oxide under the compressive strain, *i.e.*, the piezoelectric character, is one new critical material descriptor in searching for the 2DEG systems driven by the polarization discontinuity.

A good piezoelectric material should exhibit a morphotropic

phase boundary (MPB) similar to the one in the $PbZr_xTi_{1-x}O_3$, as the region near the MPB plays a critical role in creating the high electromechanical response.[40] To identify the MPB in a perovskite oxide from first-principles calculations, Ghita *et al.* proposed an approach based on the energy difference among tetragonally, rhombohedrally and rotationally distorted perovskite oxides.[41] This is because to realize a piezoelectric effect, the energy difference between these different phase structures should be as small as possible so that the continuous phase transitions over the MPB become possible.[39] In this work, all the phase structures were constructed from the optimized 5-atom cubic perovskite structure, see Figure S1 of Supporting Information. The prototype structures of tetragonal and rhombohedral phases and their distorted phases were extracted from the tetragonal $PbTiO_3$ and rhombohedral $BaTiO_3$, respectively. For rotationally distorted structures, we modeled the oxygen octahedral rotation along [111] direction in a 10-atom supercell. The ionic positions and cell shapes of all these structures were fully relaxed. The energy difference per ABO_3 unit cell among tetragonal, rhombohedral, and rotationally distorted structures is denoted as ΔE, and $\Delta E < 0.8$ eV was used as the material descriptor to identify the piezoelectric perovskite oxides. By using the energy difference among different perovskite oxide phase structures, that is, $\Delta E <$ 0.8 eV, we further narrowed down the list to from 262 to 76 candidates. In this work, we were interested in searching for the polarization-discontinuity-induced 2DEG systems based on the nonpolar/nonpolar perovskite oxide HS. This requires that both substrate and film are nonpolar oxides, *i.e.*, having a chemical formula of $A^{+2}B^{+4}O_3$, so that along [001] direction, each layer will be charge neutral. By using this condition, we ended up with 34 nonpolar piezoelectric perovskite oxides, which were used to build nonpolar/nonpolar HS systems. It is noted that the other two materials descriptors including lattice mismatch and relative band edges are determined by substrate and film together, and thus they were not used here to screen bulk perovskite oxides but used in building HS systems.

3.2 Bulk Piezoelectric Perovskite Oxides

By employing material descriptors including ΔE, E_g, and nonpolar character of perovskite oxides, we successfully obtained 34 candidate bulk piezoelectric perovskite oxides. These perovskites can be divided into six groups based on the B-site elements: Ti-, Zr-, Hf-, Si-, Ge-, and Sn-based oxides, which are listed in Table 1. For each piezoelectric perovskite oxide, we list its calculated tolerance factor (f), lattice constant a (Å), band gap E_g(eV), valence band maximum (VBM), conduction band minimum (CBM), and Born effective charge for A atom Z^*(A), B atom Z^*(B), O atom in the AO plane Z^*_{AO}(O) and O atom in the BO_2 plane $Z^*_{BO_2}$(O). The tolerance factor (t) for each selected perovskite oxide was calculated using the bond valence model:[63,64]

$$t = \frac{R_{A-O}}{\sqrt{2}(R_{B-O})} \quad (1)$$

where R_{A-O} and R_{B-O} are the A-O and B-O bond lengths for an ABO_3 compound. To have a comprehensive comparison, we calculated the lattice parameters using GGA, SCAN, and HSE approaches, respectively, along with the available experimental values. The comparison of the calculated and experimental lattice constants is presented in Figure 1. Figure 1a shows that the SCAN and HSE methods yield relatively close lattice constants, while the standard GGA approach generally overestimates the lattice constants. Figure 1b shows the former two approaches predict lattice constants much closer to the corresponding experimental values than the standard GGA approach. Considering the well-known underestimations of band gaps of insulators and semiconductors from standard GGA calculations,[65] we also calculated the band gaps of these candidate perovskites oxides using SCAN and HSE approaches. Our calculations show that the band gaps determined from the HSE approach are closer to experimental values. To characterize the relative band edge positions of these perovskite oxides, we calculated their VBM and CBM positions by aligning core levels of O ions and setting the VBM of $SrTiO_3$ as the reference zero-point energy.[17,29] As discussed later, the relative positions of the CBM can be used to justify which side of the interfacial region (film or substrate) can form the 2DEG. The

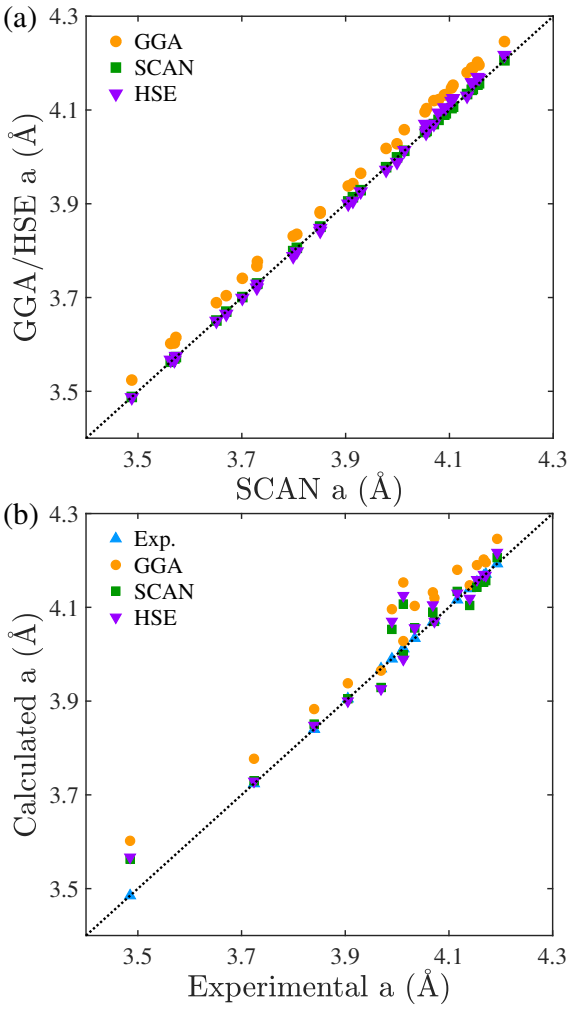

Fig. 1 (a) A comparison for the calculated lattice constants using different density functionals.(b) A comparison between experimental and theoretical lattice constants.

Table 1 Calculated properties of bulk nonpolar piezoelectric perovskites oxides (ABO_3): calculated tolerance factor t, lattice constant a(Å) and band gaps E_g(eV) from GGA, SCAN and HSE approaches, valence band maximum (VBM), conduction band minimum (CBM) and Born effective charge for A atom Z^*(A), B atom Z^*(B), O atom in the AO plane Z^*_{AO}(O) and O atom in the BO_2 plane $Z^*_{BO_2}$(O). The experimental lattice constant is also given. The * in E_g^{EXP} column indicates that the band gap was measured using an orthorhombic structure.

Compounds	t	a^{GGA}	a^{SCAN}	a^{HSE}	$a^{Exp.}$	E_g^{GGA}	E_g^{SCAN}	E_g^{HSE}	E_g^{EXP}	VBM	CBM	Z^*(A)	Z^*(B)	Z^*_{AO}(O)	$Z^*_{BO_2}$(O)	ΔH(eV)
$CaGeO_3$	0.98	3.777	3.730	3.729	3.724[42]	0.70	1.66	2.83	-	0.86	1.56	2.59	4.42	-3.58	-1.71	-4.17
$BaHfO_3$	1.01	4.196	4.157	4.168	4.171[43]	3.54	4.09	4.97	6.00[44]	-0.50	3.04	2.74	5.81	-4.56	-2.00	-5.36
$PbHfO_3$	0.95	4.147	4.104	4.119	4.140[45]	2.47	2.86	3.99	3.4[46]	-0.34	2.13	3.90	5.66	-4.60	-2.48	-4.53
$SrHfO_3$	0.95	4.132	4.090	4.105	4.069[43]	3.75	4.33	5.19	6.10[47]	-0.38	3.37	2.58	5.71	-4.58	-1.85	-5.35
$EuHfO_3$	0.96	4.127	4.083	4.105	4.088[48]	0.49	0.79	2.69	*2.7[48]	2.53	3.02	2.73	5.84	-4.50	-2.04	-5.30
$SnHfO_3$	0.90	4.133	4.093	4.105	-	1.83	2.17	3.28	-	0.00	1.83	4.29	5.63	-4.57	-2.68	-4.46
$CaHfO_3$	0.90	4.096	4.053	4.070	3.990[49]	3.68	4.28	5.18	6.20[50]	-0.40	3.28	2.63	5.63	-4.60	-1.83	-5.24
$YbHfO_3$	0.90	4.071	4.017	4.045		3.60	4.39	5.11		-0.40	3.20	2.63	5.65	-4.57	-1.85	-5.31
$CaSiO_3$	1.05	3.602	3.563	3.567	3.485[51]	3.60	4.89	5.83	-	1.25	4.85	2.61	4.13	-3.10	-1.82	-4.77
$BaSiO_3$	1.18	3.831	3.799	3.788	-	1.10	1.97	2.94	-	0.84	1.94	2.84	4.52	-3.57	-1.89	-4.41
$SrSiO_3$	1.11	3.689	3.651	3.650	-	2.56	3.73	4.74	-	1.45	4.01	2.61	4.28	-3.24	-1.82	-4.69
$GeSiO_3$	0.84	3.603	3.570	3.566	-	2.56	2.86	4.29	-	1.81	4.37	4.17	4.61	-2.98	-2.90	-3.69
$CdSiO_3$	1.02	3.615	3.573	3.575	-	0.75	1.40	2.54	-	1.72	2.47	2.79	4.18	-3.03	-1.97	-3.74
$SnSiO_3$	1.06	3.704	3.670	3.665	-	0.88	1.76	2.31	-	2.52	3.40	4.35	4.60	-3.08	-2.93	-3.74
$PbSiO_3$	1.11	3.741	3.701	3.699	-	1.31	2.35	2.95	-	1.97	3.28	4.06	4.38	-3.20	-2.62	-3.74
$MnSiO_3$	0.98	3.552	3.512	3.518	-	1.93	2.78	3.81		2.18	4.11	3.04	4.08	-2.99	-2.07	-3.84
$BaSnO_3$	1.01	4.180	4.134	4.130	4.116[43]	0.57	1.45	2.45	3.1[52]	-0.06	0.51	2.73	4.42	-3.51	-1.82	-4.20
$PbSnO_3$	0.95	4.120	4.070	4.070	4.072[53]	1.19	2.21	3.20	-	0.30	1.49	3.91	4.33	-3.25	-2.49	-3.37
$SrSnO_3$	0.96	4.103	4.056	4.056	4.034[43]	1.17	2.21	3.15	*4.1[52]	0.04	1.21	2.58	4.24	-3.32	-1.75	-4.20
$CaSnO_3$	0.90	4.058	4.013	4.014	-	1.57	2.62	3.53	*4.4[52]	0.12	1.69	2.62	4.11	-3.22	-1.75	-4.10
$GeSnO_3$	0.72	4.047	4.006	4.001	-	1.75	2.12	3.26	-	0.19	1.94	4.51	4.10	-3.11	-2.75	-3.03
$SrTiO_3$	1.00	3.938	3.905	3.900	3.905[43]	1.78	2.15	3.17	3.20[13]	0.00	1.78	2.55	7.44	-5.93	-2.03	-5.11
$BaTiO_3$	1.06	4.028	3.999	3.989	4.012[54]	1.68	2.01	2.98	3.27[55]	-0.25	1.43	2.73	7.52	-5.98	-2.13	-5.04
$PbTiO_3$	1.00	3.965	3.929	3.926	3.969[56]	1.58	1.92	2.74	3.45[57]	0.33	1.91	3.85	7.37	-6.08	-2.57	-4.25
$SnTiO_3$	0.95	3.943	3.914	3.906	-	1.05	1.31	2.15	-	0.80	1.85	4.26	7.26	-6.06	-2.73	-4.20
$GeTiO_3$	0.75	3.880	3.851	3.842	-	2.00	2.29	3.38	-	0.02	2.02	4.41	7.27	-6.09	-2.80	-3.98
$CaTiO_3$	0.95	3.883	3.851	3.848	3.840[54]	1.84	2.23	3.25	*3.8[58]	-0.02	1.82	2.57	7.38	-5.92	-2.02	-5.05
$BaZrO_3$	1.00	4.246	4.206	4.217	4.193[43]	3.06	3.69	4.44	4.85[59]	-0.67	2.39	2.72	6.23	-4.95	-2.00	-5.21
$PbZrO_3$	0.94	4.202	4.154	4.170	4.167[60]	2.33	2.71	3.88	3.72[57]	-0.69	1.64	3.89	6.06	-5.00	-2.47	-4.37
$SrZrO_3$	0.94	4.190	4.143	4.159	4.154[61]	3.24	3.91	4.65	5.60[62]	-0.57	2.67	2.57	6.12	-4.97	-1.87	-5.18
$SnZrO_3$	0.90	4.188	4.145	4.156	-	1.81	2.15	3.22	-	-0.31	1.50	4.26	6.02	-4.98	-2.65	-4.29
$EuZrO_3$	0.95	4.183	4.135	4.158	4.104[48]	0.28	0.71	2.39	*2.4[48]	2.12	2.40	2.72	6.27	-4.88	-2.06	-5.13
$CaZrO_3$	0.89	4.153	4.107	4.125	4.012[28]	3.23	3.91	4.67	*5.5[58]	-0.61	2.62	2.63	6.04	-4.98	-1.84	-5.05
$YbZrO_3$	0.90	4.131	4.071	4.101	-	3.34	3.95	4.78	-	-0.62	2.72	2.63	6.05	-4.95	-1.87	-5.11

Born effective charge for A atom Z^*(A), B atom Z^*(B), O atom in the AO plane Z^*_{AO}(O) and O atom in the BO_2 plane $Z^*_{BO_2}$(O) were also calculated to estimate the polarization strength in the HS. We noted that Ceder's team has reported bulk piezoelectric perovskite oxides using first-principles screening approach.[39] In our work, besides all the nonpolar piezoelectric perovskite oxides reported in that study, we also identified 8 more piezoelectric compounds including $CaSnO_3$, $EuHfO_3$, $EuZrO_3$, $GeSnO_3$, $GeTiO_3$, $MnSiO_3$, $YbHfO_3$, and $YbZrO_3$. Interestingly, some of these compounds have been theoretically predicted to show a polarization characteristic. For instance, $CaSnO_3$ was found to form a spontaneous polarization in its bicolor superlattice of the orthorhombic phases from first-principles calculations;[66] $GeTiO_3$ has a 137 $\mu C/cm^2$ spontaneous polarization in its rhombohedral phase.[67]

3.3 Nonpolar/Nonpolar Heterostructures

We next built all the possible nonpolar/nonpolar HS systems using the identified 34 nonpolar piezoelectric oxides and explored their possibility to form a polarization discontinuity at their interfaces. A total number of $P(34,2) = 1122$ unique oxide HS can be generated by combining the 34 selected compounds. A permutation was used here because switching the epitaxial order of the substrate and film can lead to different strain on the film (compressive strain on the film will become tensile strain if switched the growth order, and vice versa), and thus drastically change its polarization and electronic properties.[71] To form a polarization discontinuity (strictly speaking to form a polarization in the perovskite film), the oxide film needs to experience a compressive strain from the substrate, and meanwhile a small lattice mismatch between the substrate and film is desired to form an ideal perovskite oxide HS. Therefore, by defining $f = (a_f - a_s)/a_s$,[17] we only need to consider the HS with $0 < f < 6\%$, in which a positive f indicates that the film will experience a compressive strain from the substrate. By using this condition, we were able to generate 311 nonpolar/nonpolar HS systems.

To further examine whether these nonpolar/nonpolar HS systems can have polarization discontinuity and interfacial 2DEG, one needs to perform electronic structure calculations for all these HS models. However, as mentioned above, there are six groups of piezoelectric perovskite oxides according to the classification of B-site element. Hence, we selected one prototype perovskite oxide from each group as the substrate, chose all the possible piezoelectric oxides as the film using the condition of $0 < f < 6\%$, and built HS to verify the formation of polarization discontinuity at the interface. Thus, by using

Table 2 Calculated film critical thickness for polarization discontinuity induced 2DEG in substrate $SrTiO_3$-, $YbZrO_3$-, $CaHfO_3$-, $BaSiO_3$-, $CaGeO_3$-, and $SrSnO_3$-based HS. f is the lattice mismatch between the substrate and film; t_c is the film critical thickness once polarization is formed in the film layers; $t_c^{'}$ is the film critical thickness once the polarization state is energetic more favorable than the paraelectric state. The * indicates that a HS has been experimentally validated.

$SrTiO_3$				$YbZrO_3$				$CaHfO_3$				$BaSiO_3$				$CaGeO_3$				$SrSnO_3$			
Film	$f(\%)$	t_c	$t_c^{'}$	Film	$f(\%)$	t_c	$t_c^{'}$	Film	$f(\%)$	t_c	$t_c^{'}$	Film	$f(\%)$	t_c	$t_c^{'}$	Film	$f(\%)$	t_c	$t_c^{'}$	Film	$f(\%)$	t_c	$t_c^{'}$
$SnTiO_3$	0.14	6	7	$SrHfO_3$	0.02	-	-	$SrSnO_3$	0.17	-	-	$GeTiO_3$	1.26	2	3	$BaSiO_3$	1.45	2	2	$PbSnO_3$	0.41	8	13
*$PbTiO_3$ [30]	0.69	9	12	$SnHfO_3$	0.05	4	7	$PbSnO_3$	0.58	10	-	$CaTiO_3$	1.34	6	11	$GeTiO_3$	2.72	3	4	$EuHfO_3$	0.58	2	2
*$BaTiO_3$ [68]	2.29	4	4	$PbHfO_3$	0.39	8	12	$EuHfO_3$	0.76	2	2	$SrTiO_3$	2.78	5	10	$CaTiO_3$	2.81	4	5	$YbZrO_3$	0.68	3	4
$GeSnO_3$	2.77	2	3	$CaZrO_3$	0.53	3	5	$YbZrO_3$	0.85	4	5	$SnTiO_3$	2.92	3	3	$SrTiO_3$	4.26	2	2	$SrHfO_3$	0.69	-	-
$CaSnO_3$	3.05	5	7	$BaSnO_3$	1.19	-	-	$SrHfO_3$	0.87	-	-	$PbTiO_3$	3.48	4	8	$SnTiO_3$	4.41	3	3	$SnHfO_3$	0.73	5	6
$YbHfO_3$	3.38	3	3	$EuZrO_3$	1.26	2	2	$SnHfO_3$	0.91	6	7	$BaTiO_3$	5.13	3	4	$PbTiO_3$	4.98	3	3	$PbHfO_3$	1.06	7	9
*$CaHfO_3$ [69]	4.03	3	4	$SnZrO_3$	1.38	3	5	$PbHfO_3$	1.24	10	13	$GeSnO_3$	5.64	2	2	-	-	-	-	$CaZrO_3$	1.20	3	5
$SrSnO_3$	4.21	-	-	$SrZrO_3$	1.43	8	13	$CaZrO_3$	1.37	5	6	$CaSnO_3$	5.92	3	4	-	-	-	-	$BaSnO_3$	1.86	-	-
$PbSnO_3$	4.63	7	7	$BaHfO_3$	1.57	-	-	$BaSnO_3$	2.04	-	-	-	-	-	-	-	-	-	-	$EuZrO_3$	1.95	2	2
$EuHfO_3$	4.80	2	2	$PbZrO_3$	1.72	5	7	$EuZrO_3$	2.12	2	-	-	-	-	-	-	-	-	-	$SnZrO_3$	2.06	3	5
$YbZrO_3$	4.90	2	2	$BaZrO_3$	2.78	-	-	$SnZrO_3$	2.24	4	5	-	-	-	-	-	-	-	-	$SrZrO_3$	2.10	6	11
$SrHfO_3$	4.93	4	6	-	-	-	-	$SrZrO_3$	2.28	12	15	-	-	-	-	-	-	-	-	$BaHfO_3$	2.26	-	-
$SnHfO_3$	4.97	3	3	-	-	-	-	$BaHfO_3$	2.44	-	-	-	-	-	-	-	-	-	-	$PbZrO_3$	2.40	5	7
$PbHfO_3$	5.32	4	4	-	-	-	-	$PbZrO_3$	2.58	7	8	-	-	-	-	-	-	-	-	$BaZrO_3$	3.48	9	12
*$CaZrO_3$ [28]	5.46	2	5	-	-	-	-	$BaZrO_3$	3.66	-	-	-	-	-	-	-	-	-	-	-	-	-	-
*$BaSnO_3$ [70]	6.15	6	-	-	-	-	-	-	-	-	-	-	-	-	-	-	-	-	-	-	-	-	-

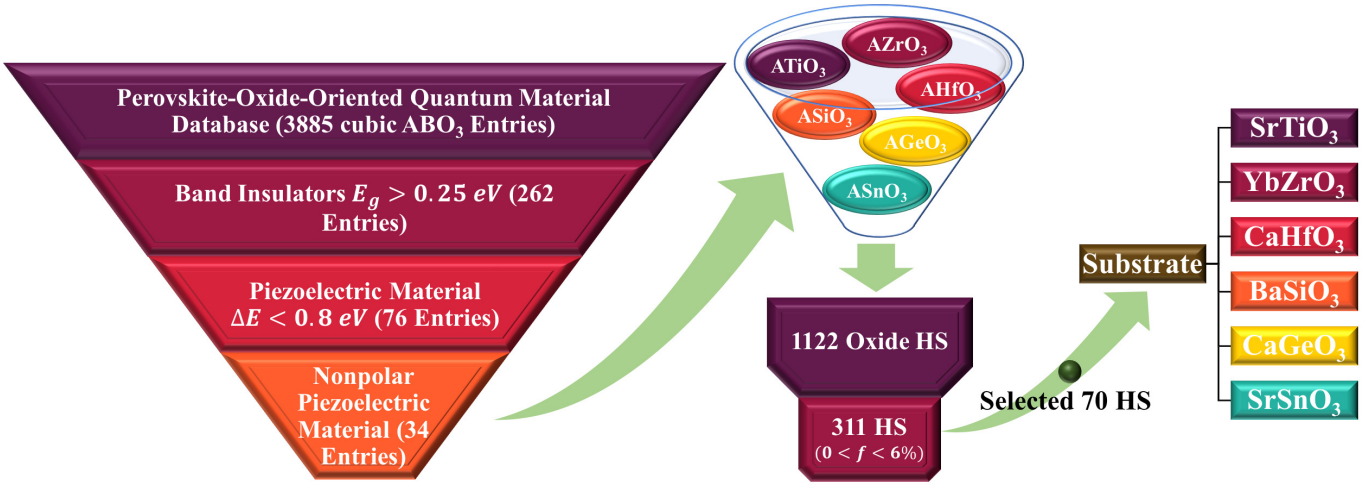

Fig. 2 Flowchart summary of high-throughput screening and elimination procedure in this study, from first identifying all the possible nonpolar piezoelectric perovskite oxides to constructing all the candidate nonpolar/nonpolar HS and then to verifying the existence of 2DEG in 70 selected HS.

$SrTiO_3$, $YbZrO_3$, $CaHfO_3$, $BaSiO_3$, $CaGeO_3$, and $SrSnO_3$ as the substrate, we were able to generate a total number of 70 HS systems in six groups, see Table 2. This strategy can significantly reduce computational cost of HS models from 311 to 70, and meanwhile give reliable sample evaluation of the interfacial materials properties of all the HS models. A complete screening and elimination procedure is shown in Fig. 2. A series of prior experimental and computational studies show that there exists a critical film thickness to form a polarization discontinuity in the nonpolar/nonpolar HS.[15,28,29] Here, we define t_c as the film critical thickness once polarization is formed in the film layers and $t_c^{'}$ as the film critical thickness once the polarization state is energetic more favorable than its paraelectric state. In other words, the $t_c^{'}$ is the critical film thickness to form a stable polarization state. The t_c and $t_c^{'}$ are listed in the Table 2. Also note that the lattice-mismatch-induced polarization can point towards either the interface or the surface of the film, *i.e.*, the vacuum, and only a strong enough polarization towards the interface can drive the charge transfer from the film to the substrate, and produce the interfacial 2DEG. In contrast, a strong polarization towards the surface will drive the charge transfer from the substrate to the film, and produce the interfacial two-dimensional hole gas (2DHG), as discussed later. In Table 2, we list all the possible oxide films that can form a polarization discontinuity and 2DEG at the interface for each selected substrate. 13 exceptional HS systems that cannot form interfacial metallic states, even the film thickness was increased up to 15 unit cells, include: $SrSnO_3/SrTiO_3$, $SrHfO_3/YbZrO_3$, $BaSnO_3/YbZrO_3$, $BaHfO_3/YbZrO_3$, $BaZrO_3/YbZrO_3$, $SrSnO_3/CaHfO_3$, $SrHfO_3/CaHfO_3$, $BaSnO_3/CaHfO_3$, $BaHfO_3/CaHfO_3$, $BaZrO_3/CaHfO_3$, $SrHfO_3/SrSnO_3$, $BaSnO_3/SrSnO_3$ and $BaHfO_3/SrSnO_3$.

In addition, we also found a correlation between critical film thickness t_c and lattice mismatch f in the $SrTiO_3$- and $BaSiO_3$-based HS. That is, a large f corresponds to a small t_c, as in the case of our prior study of $AHfO_3/SrTiO_3$ (A = Ca, Sr, and Ba) HS.[29] This is because as f increases, the film will experience a higher compression strain from the substrate so that the

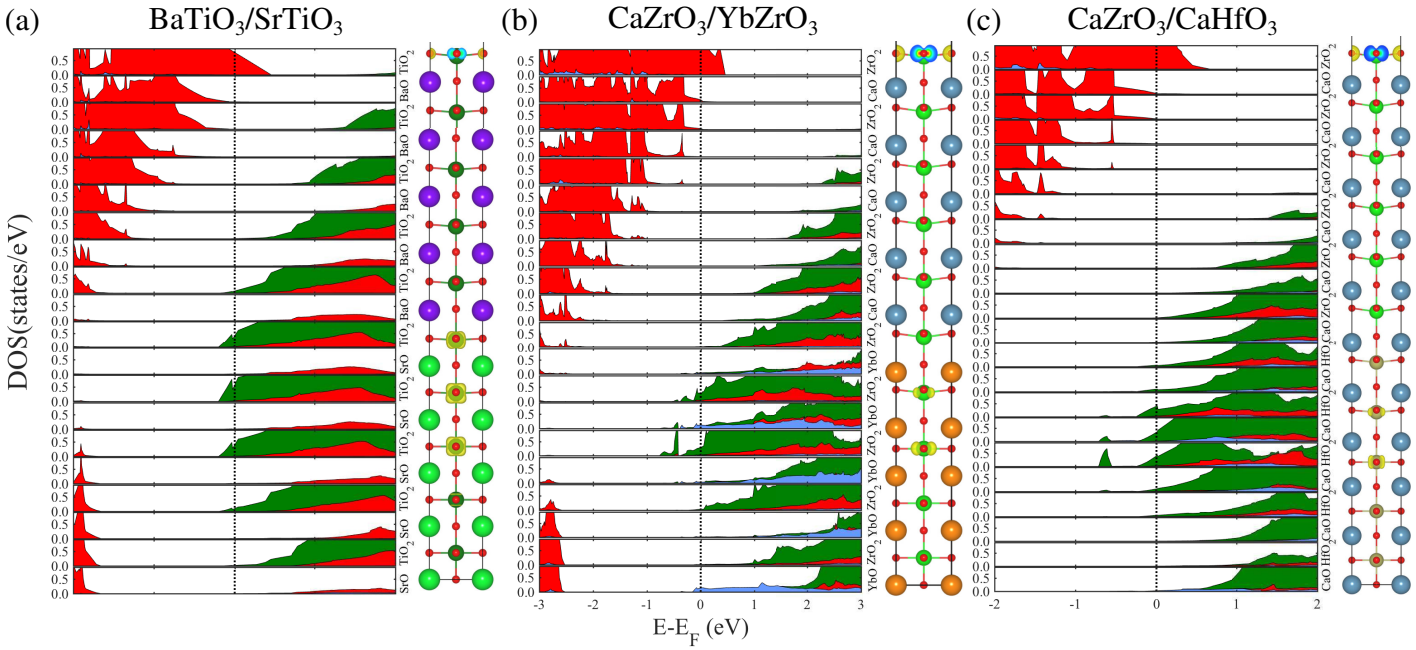

Fig. 3 Calculated layer-resolved partial DOS for (a) $BaTiO_3/SrTiO_3$, (b) $CaZrO_3/YbZrO_3$ and (c) $CaZrO_3/CaHfO_3$ HS, along with their charge density plots projected on the bands forming the metallic states. The vertical dash line at zero point energy shows the Fermi level. The solid blue, red, and green color indicates *s*, *p* and *d* orbital, respectively.

film tends to exhibit polarization with a smaller t_c. Also, interestingly, when the A-site element in the film of the HS is Eu, Yb, Ge, or Sn, for example, the HS systems $EuZrO_3/SrSnO_3$, $YbZrO_3/SrSnO_3$, $GeTiO_3/BaSiO_3$, and $SnTiO_3/SrTiO_3$, the HS needs a much smaller t_c to form the polarization. In particular, when $EuZrO_3$ and $EuHfO_3$ serve as the film to form a HS, the critical film thickness to form a polarization is as low as two unit cells, regardless of the f value. Accordingly, except for the lattice mismatch f, the A-site element such as Eu, Yb, Ge, or Sn also plays a significant role in determining t_c. However, it is noted that a strain-induced polarization is essentially determined by its energy preference over non-polarized state. By taking $BaTiO_3/SrTiO_3$ HS models (with different film thickness) as an example, we have calculated its total energy per unit cell (of the film) as a function of the average polarization, see Figure S2 of the Supporting Information. It clearly shows that the ground state of $BaTiO_3/SrTiO_3$ becomes polarized as the film thickness is larger than 4 unit cells, *i.e.*, $t_c = 4$.

Next, to clearly show the polarization behavior in the oxide film and the charge transfer mechanism in these HS models, we selected one HS model from each group of the materials systems in Table 2 and plotted their layer-resolved density of states (DOS) and three-dimensional (3D) charge density projected on their conduction bands forming the interfacial metallic states, as shown in Figure 3 and 4. Figure 3 shows the results for $BaTiO_3/SrTiO_3$, $CaZrO_3/YbZrO_3$ and $CaZrO_3/CaHfO_3$, and Figure 4 shows the results for $CaSnO_3/BaSiO_3$, $BaSiO_3/CaGeO_3$ and $CaZrO_3/SrSnO_3$. The layer-resolved DOS show that the O 2*p* states in all these systems move to higher energy states from the interfacial layer to the surface layer, and at the surface layer, some O 2*p* states cross the Fermi level and become unoccupied. This indicates that there exists an intrinsic electric field, which is caused by the relative cation-anion displacement in the oxide films, that is, the polarization towards the interface, as shown in the corresponding geometrical structures. Also note that the relative displacement between cations and anions in each substrate material is much smaller than that in its corresponding film, implying that a polarization discontinuity is formed at the interface, which is caused by the lattice-mismatch-induced compressive strain on the oxide films. Moreover, at interfacial layers, some bottom conduction bands cross the Fermi level and form the interfacial conductivity, as shown in the 3D charge density plot. This suggests that the polarization discontinuity at the interface leads to the charge transfer from the film to the substrate, and these transferred electrons generally reside near the interfacial region of the substrate, forming the interfacial conductivity. For $BaTiO_3/SrTiO_3$, $CaZrO_3/YbZrO_3$, and $CaZrO_3/CaHfO_3$ HS, their interfacial metallic states are mainly contributed from Ti 3*d*, Zr 4*d*, and Hf 5*d* orbitals, respectively, see Figure 3(a-c). For $CaSnO_3/BaSiO_3$, $BaSiO_3/CaGeO_3$, and $CaZrO_3/SrSnO_3$ systems, their interfacial metallic states are mainly from Si 3*s*, Ge 4*s*, and Sn 5*s* orbitals, respectively, as shown by the solid blue in Figure 4(a-c). We then calculated the effective mass values for the 6 exemplary HS by fitting their electronic bands contributing to the 2DEG, see Figure 5 and Table S1 of the Supporting Information. We found that the effective mass for $CaSnO_3/BaSiO_3$, $BaSiO_3/CaGeO_3$ and $CaZrO_3/SrSnO_3$ ($m^* \approx 0.3m_e$) are generally smaller than that in $BaTiO_3/SrTiO_3$, $CaZrO_3/YbZrO_3$ and $CaZrO_3/CaHfO_3$ HS ($m^* \approx 0.4-0.5m_e$) because of a more delocalization character of *s* orbital than that of *d* orbitals.[72] Hence, a high electron mobility is expected in Si-, Ge-, and Sn-based 2DEG HS.

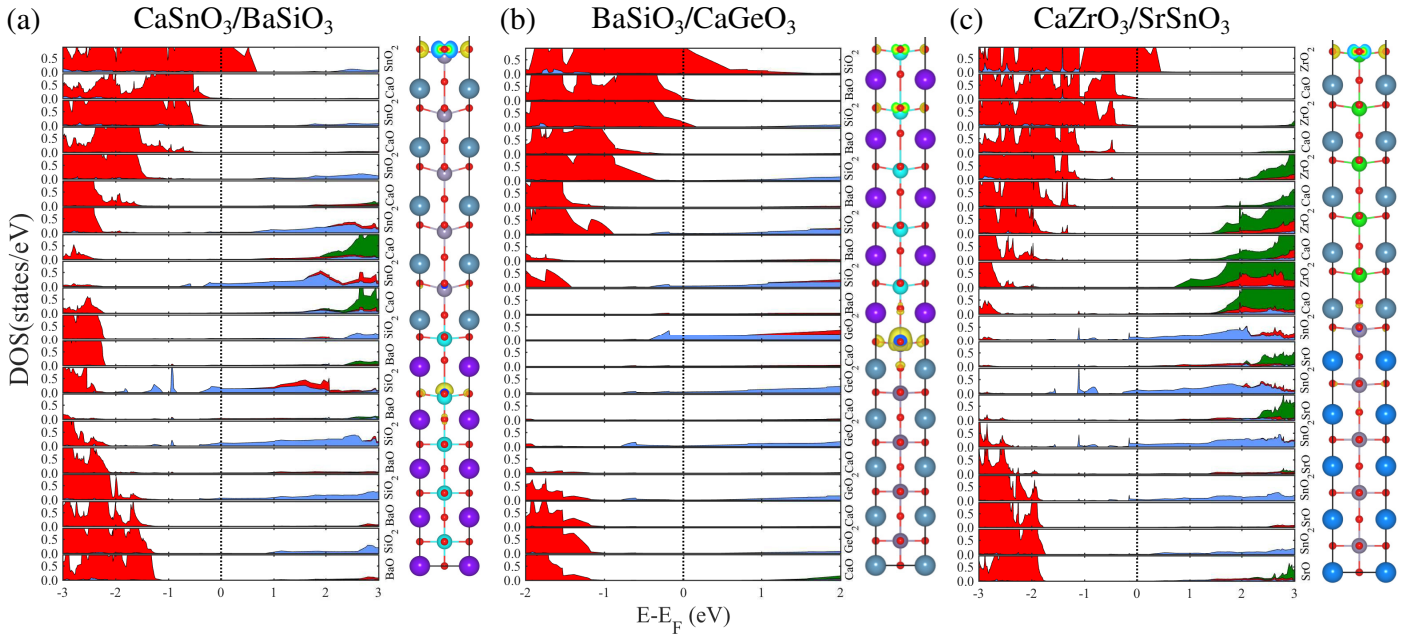

Fig. 4 Calculated layer-resolved partial DOS for (a) $CaSnO_3/BaSiO_3$, (b) $BaSiO_3/CaGeO_3$ and (c) $CaZrO_3/SrSnO_3$ HS, along with their charge density plots projected on the bands forming the metallic states.

Moreover, it is worth mentioning that, in the $CaSnO_3/BaSiO_3$ HS, some interfacial layers in the film also contribute to the interfacial metallic states, which indicates that the transferred electrons, from the film to the substrate driven by the polarization discontinuity, partially flow back to the film. The underlying mechanism of this intriguing phenomenon can be rationalized in terms of the band alignment between the film and substrate. In our prior work of high-throughput design of perovskite-oxide-based 2DEG systems based on the polar catastrophe, we defined one material descriptor, *i.e.*, the band alignment between the film and substrate, to characterize the charge transfer from the film to the substrate driven by the polar catastrophe, and the resulting 2DEG at the interface.[17,29] In the polar catastrophe mechanism, CBM of the polar film (electron donor) should be higher than that of the nonpolar substrate (acceptor), so that electrons can be confined at the side of the electron-acceptor material and form the interfacial metallic states; otherwise, the interfacial metallic states cannot be formed. However, in the nonpolar/nonpolar interface system, the donor electrons, caused by the polarization discontinuity, can form metallic states near the interfacial region in both the film and substrate since they are originally nonpolar (not charged). For the $CaSnO_3/BaSiO_3$ system, as shown in Table 1, the CBM of film $CaSnO_3$ is lower than that of the substrate $BaSiO_3$. After electronic reconstruction at the interface, the lower energy states at the interfacial region are both from the film and substrate, and accordingly, when the electrons are transferred from the film to the substrate via the intrinsic electric field in the film, the electrons tend to stay at a lower energy state and thus partial electrons flow back to the film. Thus, the 2DEG are contributed both from the interfacial layers in the substrate and film. For some HS, such as $SrTiO_3/SrSiO_3$ and $BaTiO_3/BaSiO_3$, the film CBM is significantly lower than that of the substrate, and even after electronic reconstruction, the film CBM is still much lower than that of the substrate, then the transferred electron will be solely accumulated in the film side near the interfacial region. Therefore, the 2DEG forms in the film side of the interfacial region, see the calculated layer-resolved DOS of these two systems in Figure S3 of the Supporting Information. In contrast, when a film CBM is much higher than that of the substrate, there will be no electrons flowing back and the 2DEG only appear in the substrate side of the interfacial region, such as $CaZrO_3/SrSnO_3$ systems.

3.4 Polarization Robustness

In this section, we explored the polarization robustness in these nonpolar/nonpolar HS. Here we started by investigating the polarization stability and switching path in these systems, as various ferroelectric phase transitions have been found in the ferroelectric HS.[73–75] In our calculations, the first two unit cells of the substrate and all the film layers were initialized as polarized, with a small relative displacement between cations and their neighbor oxygen anions in the same plane. The initial polarization was set as either toward the interface (P_+) or toward the vacuum (P_-), and then a structural relaxation was carried out to examine the polarization stability. That is, whether the polarization can persist in the ground state optimized structure. If the polarization remains after structural relaxation, then it is stable, otherwise not stable and cannot be formed. If both the P_- and P_+ polarization cannot be formed, then the HS is intrinsically paraelectric, as discussed later in the case of $SrHfO_3/CaHfO_3$. It is worth mentioning that when polarization is switched from P_+ to P_-, the interfacial metallic states will be changed from 2DEG to 2DHG, as shown in Figure S4 of Supporting Information. Accordingly, further experimental studies are worth being done to verify the formation of 2DHG. In fact, recently, a 2DHG has been experi-

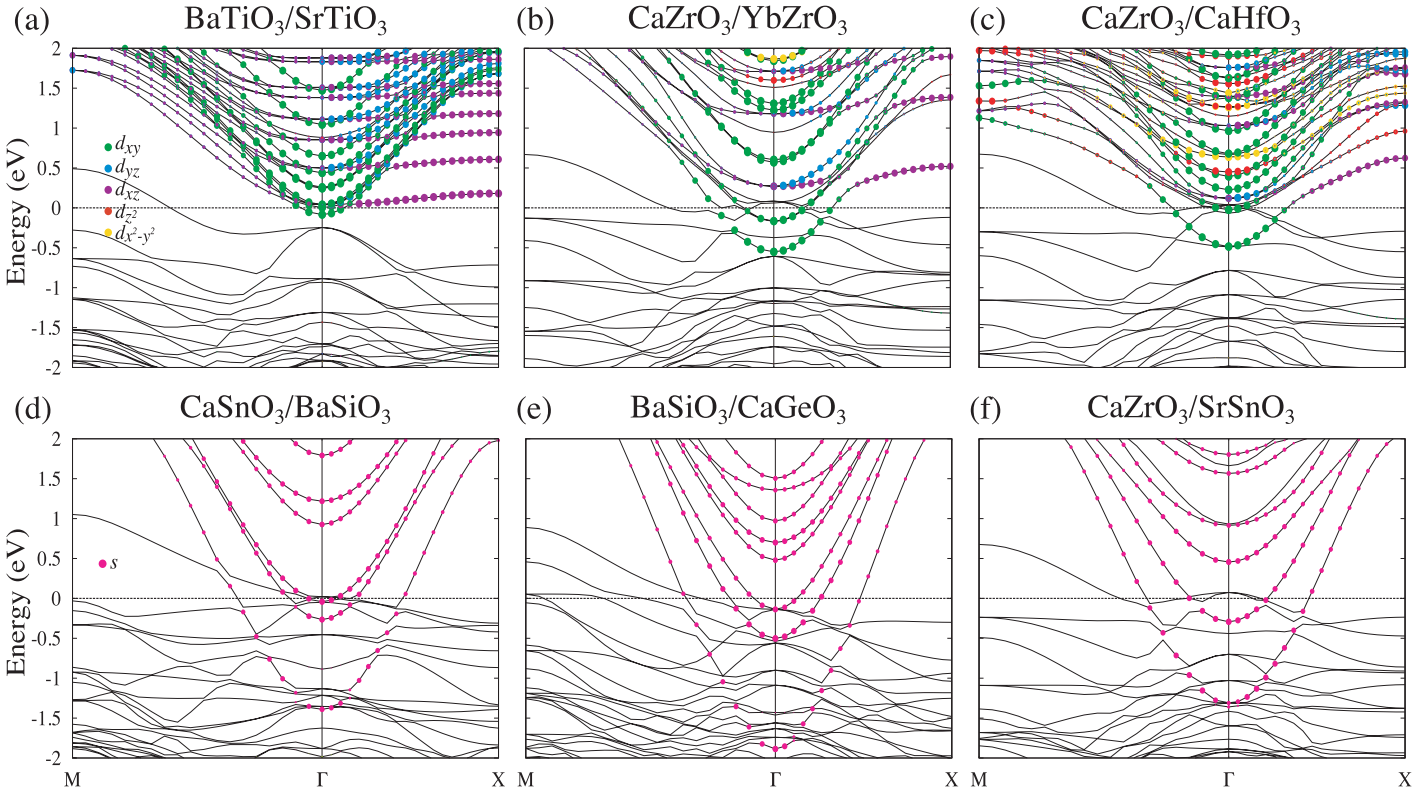

Fig. 5 Orbital projected band structures for (a) $BaTiO_3/SrTiO_3$, (b) $CaZrO_3/YbZrO_3$, (c) $CaZrO_3/CaHfO_3$, (d) $CaSnO_3/BaSiO_3$, (e) $BaSiO_3/CaGeO_3$, and (f) $CaZrO_3/SrSnO_3$ HS. The horizontal dot line indicates the Fermi level at zero.

mentally observed in the p-type polar/nonpolar $LaAlO_3/SrTiO_3$ interface,[76,77] in which the 2DHG was attributed to the *p*-type $(AlO_2)^-/(SrO)^0$ interface rather than the polarization discontinuity.

Next, to determine the polarization switching behavior and potential energy barrier between different polarization states, we calculated the energy versus polarization ($E(P)$) profiles for all the HS systems in the Table 2 by interpolating continuously between paraelectric and ferroelectric states.[73,74,78] The average polarization of each unit cell in the film was calculated using the following formula:[79,80]

$$P = \frac{e}{\Omega}\sum_{i=1}^{N} Z_i^* \delta z_i \qquad (2)$$

in which Ω and N are the average volume and number of ions in one unit cell, respectively, Z_i^* is the Born effective charge for each ion, and δz_i is the displacement of the ith atom away from its original position in paraelectric phase. Based on the obtained $E(P)$ curves, we were able to further divide the $E(P)$ profiles into five different types, according to the spontaneous polarization direction and the relative stability of paraelectric and ferroelectric states, see Talbe 3. Note that the $E(P)$ curve for each HS was calculated at the critical film thickness t_c of forming polarization state, and as the film thickness further increases, the $E(P)$ curve could be changed to a different type. To clearly show the polarization behaviors and classification of $E(P)$ curves of these HS systems, we selected five types of HS systems based on their $E(P)$ characters, and showed their $E(P)$ profiles in Figure 6. Several conclusions can be derived as below:

i) For the first two types of $E(P)$ profiles, *i.e.*, Type-1 for $(SrHfO_3)_6/CaHfO_3$ and Type-2 for $(SrTiO_3)_5/CaGeO_3$, there exists only one local energy minimum, which is also the global energy minimum, see Figure 6(a, b). In other words, there are no metastable polarization states. For $(SrHfO_3)_6/CaHfO_3$, its ground state is non-polarized and no stable polarization state exists in the HS, while for $(SrTiO_3)_5/CaGeO_3$, its ground state has a spontaneous P_+ with a polarization direction towards the interface.

ii) For the third and fourth types of $E(P)$ profiles, *i.e.*, Type-3 for $(CaHfO_3)_4/SrTiO_3$ and Type-4 for $(PbSnO_3)_{12}/CaHfO_3$, they show an asymmetric-like double-well $E(P)$ curve, see Figure 6(c, d). This indicates that there exist one metastable state (local energy minimum) and one ground state (global energy minimum) in these systems. For $(CaHfO_3)_4/SrTiO_3$, its metastable state is non-polarized while ground state has a P_+ state towards $SrTiO_3$ substrate. This means that without an initial P_+ configuration, the HS with a Type-3 $E(P)$ character will remain non-polarized due to an energy barrier from the metastable P_0 to the ground-state P_+ (about 15 meV). Also, there is no stable P_- state in Type-3, which means even if the HS is initially with a P_- configuration, the initial polarization will eventually disappear after structural relaxation and the system becomes non-polarized. On the other hand, the HS systems with a Type-4 $E(P)$ character can exhibit a spontaneous P_- polarization and an energy barrier must be overcome to have a transition from P_- state to P_+ state in Type-4 systems.

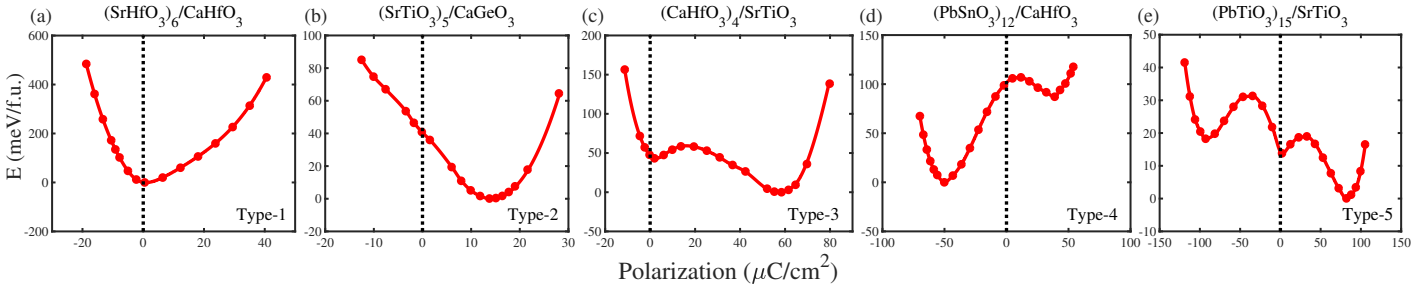

Fig. 6 Calculated total energy per film unit cell as a function of the average polarization for (a) $(SrHfO_3)_6/CaHfO_3$, (b) $(SrTiO_3)_5/CaGeO_3$, (c) $(CaHfO_3)_4/SrTiO_3$, (d) $(PbSnO_3)_{12}/CaHfO_3$, and (e) $(PbTiO_3)_{15}/SrTiO_3$ HS. The lowest total energies of each system are taken as the reference energies.

Table 3 Polarization types for substrate $SrTiO_3$-, $YbZrO_3$-, $CaHfO_3$-, $BaSiO_3$-, $CaGeO_3$- and $SrSnO_3$-based HS. The polarization type for each HS system is determined at t_c film critical thickness, which means it is evaluated once polarization is formed in the film layers. Note that the polarization type can be changed to another type if film thickness is further increased.

Type-1	Type-2	Type-3	Type-4	Type-5
$SrSnO_3/SrTiO_3$	$BaTiO_3/SrTiO_3$	$GeSnO_3/SrTiO_3$	$EuZrO_3/YbZrO_3$	$SnTiO_3/SrTiO_3$
$SrHfO_3/YbZrO_3$	$EuHfO_3/SrTiO_3$	$YbHfO_3/SrTiO_3$	$PbSnO_3/CaHfO_3$	$PbTiO_3/SrTiO_3$
$BaSnO_3/YbZrO_3$	$SnTiO_3/BaSiO_3$	$CaHfO_3/SrTiO_3$	$EuHfO_3/CaHfO_3$	$CaSnO_3/SrTiO_3$
$BaHfO_3/YbZrO_3$	$BaSiO_3/CaGeO_3$	$YbZrO_3/SrTiO_3$	$EuZrO_3/CaHfO_3$	$PbSnO_3/SrTiO_3$
$BaZrO_3/YbZrO_3$	$SrTiO_3/CaGeO_3$	$SrHfO_3/SrTiO_3$	-	$BaSnO_3/SrTiO_3$
$SrSnO_3/CaHfO_3$	$SnTiO_3/CaGeO_3$	$SnHfO_3/SrTiO_3$	-	$PbSnO_3/SrSnO_3$
$SrHfO_3/CaHfO_3$	$PbTiO_3/CaGeO_3$	$PbHfO_3/SrTiO_3$	-	-
$BaSnO_3/CaHfO_3$	$EuHfO_3/SrSnO_3$	$CaZrO_3/SrTiO_3$	-	-
$BaHfO_3/CaHfO_3$	$EuZrO_3/SrSnO_3$	$SnHfO_3/YbZrO_3$	-	-
$BaZrO_3/CaHfO_3$	-	$PbHfO_3/YbZrO_3$	-	-
$SrHfO_3/SrSnO_3$	-	$CaZrO_3/YbZrO_3$	-	-
$BaSnO_3/SrSnO_3$	-	$SnZrO_3/YbZrO_3$	-	-
$BaHfO_3/SrSnO_3$	-	$SrZrO_3/YbZrO_3$	-	-
-	-	$PbZrO_3/YbZrO_3$	-	-
-	-	$YbZrO_3/CaHfO_3$	-	-
-	-	$SnHfO_3/CaHfO_3$	-	-
-	-	$PbHfO_3/CaHfO_3$	-	-
-	-	$CaZrO_3/CaHfO_3$	-	-
-	-	$SnZrO_3/CaHfO_3$	-	-
-	-	$SrZrO_3/CaHfO_3$	-	-
-	-	$PbZrO_3/CaHfO_3$	-	-
-	-	$GeTiO_3/BaSiO_3$	-	-
-	-	$CaTiO_3/BaSiO_3$	-	-
-	-	$SrTiO_3/BaSiO_3$	-	-
-	-	$PbTiO_3/BaSiO_3$	-	-
-	-	$BaTiO_3/BaSiO_3$	-	-
-	-	$CaSnO_3/BaSiO_3$	-	-
-	-	$GeSnO_3/BaSiO_3$	-	-
-	-	$GeTiO_3/CaGeO_3$	-	-
-	-	$CaTiO_3/CaGeO_3$	-	-
-	-	$YbZrO_3/SrSnO_3$	-	-
-	-	$SnHfO_3/SrSnO_3$	-	-
-	-	$PbHfO_3/SrSnO_3$	-	-
-	-	$CaZrO_3/SrSnO_3$	-	-
-	-	$SnZrO_3/SrSnO_3$	-	-
-	-	$SrZrO_3/SrSnO_3$	-	-
-	-	$PbZrO_3/SrSnO_3$	-	-
-	-	$BaZrO_3/SrSnO_3$	-	-

iii) For the fifth type of $E(P)$ profile, *i.e.*, Type-5 for $(PbTiO_3)_{15}/SrTiO_3$, it has three local energy minimums at P_-, P_0, and P_+, and the global energy minimum has a P_+ towards the $SrTiO_3$ substrate. The energy barrier is about 5.15 meV from P_0 to P_+ and about 17.51 meV from P_0 to P_-. To reach the ground state (with P_+) or the metastable state (with P_-), an initial polarization must be set to overcome the energy barrier.

4 Conclusion

In conclusion, we have demonstrated a high-throughput computational approach to design polarization-discontinuity-induced 2DEG systems at perovskite-oxide-based nonpolar/nonpolar interfaces. Based on a large quantum materials repository of ABO_3 chemical space, and by employing a group of combinatorial materials descriptors based on the band gap and energy proximity among different perovskite phases, we were able to identify 34 nonpolar piezoelectric perovskite oxides, which can be further divided into six groups of materials based on B-site elements: Ti-, Zr-, Hf-, Si-, Ge- and Sn-based oxides. From the 34 selected piezoelectric compounds, we have constructed 311 nonpolar/nonpolar HS, based on the requirement of the lattice mismatch between the film and substrate in the range of $0 < f < 6\%$. By taking $SrTiO_3$-, $YbZrO_3$-, $CaHfO_3$-, $BaSiO_3$-, $CaGeO_3$- and $SrSnO_3$-based HS as the exemplary models, we calculated electronic structures of 70 selected HS, and verified the formation of 2DEG at the interface. The critical thickness to form interfacial 2DEG and the energy versus polarization profiles of each HS system were also studied. This work provides a platform to accelerate the design of perovskite-oxide-based interface materials.

5 Acknowledgment

This work was partially supported by the National Science Foundation under award number ACI-1550404 and the Vannevar Bush Faculty Fellowship program sponsored by the Basic Research Office of the Assistant Secretary of Defense for Research and Engineering (under the Office of Naval Research grant N00014-16-1-2569). This work used the Extreme Science and Engineering Discovery Environment (XSEDE), which is supported by National Science Foundation grant number OCI-1053575.

6 Data availability

The raw/processed data required to reproduce these findings cannot be shared at this time due to technical or time limitations.

Notes and references

1 M. Gibert, P. Zubko, R. Scherwitzl, J. Íñiguez and J.-M. Triscone, *Nat. Mater.*, 2012, **11**, 195.

2 H. Zhang, H. Zhang, X. Yan, X. Zhang, Q. Zhang, J. Zhang, F. Han, L. Gu, B. Liu, Y. Chen, B. Shen and J. Sun, *ACS Appl. Mater. Interfaces*, 2017, **9**, 36456–36461.

3 N. Reyren, M. Bibes, E. Lesne, J.-M. George, C. Deranlot, S. Collin, A. Barthélémy and H. Jaffrès, *Phys. Rev. Lett.*, 2012, **108**, 186802.

4 M. Lorenz, M. S. R. Rao, T. Venkatesan, E. Fortunato, P. Barquinha, R. Branquinho, D. Salgueiro, R. Martins, E. Carlos, A. Liu, F. K. Shan, M. Grundmann, H. Boschker, J. Mukherjee, M. Priyadarshini, N. DasGupta, D. J. Rogers, F. H. Teherani, E. V. Sandana, P. Bove, K. Rietwyk, A. Zaban, A. Veziridis, A. Weidenkaff, M. Muralidhar, M. Murakami, S. Abel, J. Fompeyrine, J. Zuniga-Perez, R. Ramesh, N. A. Spaldin, S. Ostanin, V. Borisov, I. Mertig, V. Lazenka, G. Srinivasan, W. Prellier, M. Uchida, M. Kawasaki, R. Pentcheva, P. Gegenwart, F. M. Granozio, J. Fontcuberta and N. Pryds, *J. Phys. D: Appl. Phys.*, 2016, **49**, 433001.

5 M. Brahlek, A. S. Gupta, J. Lapano, J. Roth, H.-T. Zhang, L. Zhang, R. Haislmaier and R. Engel-Herbert, *Adv. Fun. Mater.*, 2017, **28**, 1702772.

6 P. Zubko, S. Gariglio, M. Gabay, P. Ghosez and J.-M. Triscone, *Annu. Rev. Condens. Matter Phys.*, 2011, **2**, 141–165.

7 F. Trier, G. E. D. K. Prawiroatmodjo, Z. Zhong, D. V. Christensen, M. von Soosten, A. Bhowmik, J. M. G. Lastra, Y. Chen, T. S. Jespersen and N. Pryds, *Phys. Rev. Lett.*, 2016, **117**, 096804.

8 Y. Matsubara, K. S. Takahashi, M. S. Bahramy, Y. Kozuka, D. Maryenko, J. Falson, A. Tsukazaki, Y. Tokura and M. Kawasaki, *Nat. Commun.*, 2016, **7**, 11631.

9 N. Reyren, S. Thiel, A. D. Caviglia, L. F. Kourkoutis, G. Hammer, C. Richter, C. W. Schneider, T. Kopp, A. S. Rüetschi, D. Jaccard, M. Gabay, D. A. Muller, J. M. Triscone and J. Mannhart, *Science*, 2007, **317**, 1196–1199.

10 B. Kalisky, J. A. Bert, B. B. Klopfer, C. Bell, H. K. Sato, M. Hosoda, Y. Hikita, H. Y. Hwang and K. A. Moler, *Nat. Commun.*, 2012, **3**, 922.

11 G. Cheng, P. F. Siles, F. Bi, C. Cen, D. F. Bogorin, C. W. Bark, C. M. Folkman, J.-W. Park, C.-B. Eom, G. Medeiros-Ribeiro and J. Levy, *Nat. Nanotechnol.*, 2011, **6**, 343.

12 E. Lesne, Y. Fu, S. Oyarzun, J. C. Rojas-Sánchez, D. C. Vaz, H. Naganuma, G. Sicoli, J.-P. Attané, M. Jamet, E. Jacquet, J.-M. George, A. Barthélémy, H. Jaffrès, A. Fert, M. Bibes and L. Vila, *Nat. Mater.*, 2016, **15**, 1261.

13 A. Ohtomo and H. Y. Hwang, *Nature*, 2004, **427**, 423–426.

14 M. Behtash, S. Nazir, Y. Wang and K. Yang, *Phys. Chem. Chem. Phys.*, 2016, **18**, 6831–6838.

15 S. Nazir, J. Cheng and K. Yang, *ACS Appl. Mater. Interfaces*, 2016, **8**, 390–399.

16 Y. Wang, W. Tang, J. Cheng, M. Behtash and K. Yang, *ACS Appl. Mater. Interfaces*, 2016, **8**, 13659–13668.

17 K. Yang, S. Nazir, M. Behtash and J. Cheng, *Sci. Rep.*, 2016, **6**, 34667.

18 M. P. Warusawithana, C. Richter, P. Roy, J. Ludwig, S. Paetel, T. Heeg, A. A. Pawlicki, L. F. Kourkoutis, M. Zheng, M. Lee, B. Mulcahy, W. Zander, Y. Zhu, J. Schubert, J. N. Eckstein, D. A. Muller, C. S. Hellberg, J. Mannhart and D. G. Schlom, *Nat. Commun.*, 2013, **4**, 2351.

19 Z. Liu, C. Li, W. Lü, X. Huang, Z. Huang, S. Zeng, X. Qiu, L. Huang, A. Annadi, J. Chen, J. Coey, T. Venkatesan and Ariando, *Phys. Rev. X*, 2013, **3**, 021010.

20 L. Yu and A. Zunger, *Nat. Commun.*, 2014, **5**, 5118.

21 N. Nakagawa, H. Y. Hwang and D. A. Muller, *Nat. Mater.*, 2006, **5**, 204–209.

22 S. A. Pauli, S. J. Leake, B. Delley, M. Björck, C. W. Schneider, C. M. Schlepütz, D. Martoccia, S. Paetel, J. Mannhart and P. R. Willmott, *Phys. Rev. Lett.*, 2011, **106**, 036101.

23 S. Ryu, H. Zhou, T. R. Paudel, J. Irwin, J. P. Podkaminer, C. W. Bark, D. Lee, T. H. Kim, D. D. Fong, M. S. Rzchowski, E. Y. Tsymbal and C. B. Eom, *Appl. Phys. Lett.*, 2017, **111**, 141604.

24 J. Biscaras, N. Bergeal, A. Kushwaha, T. Wolf, A. Rastogi, R. Budhani and J. Lesueur, *Nat. Commun.*, 2010, **1**, 89.

25 P. Moetakef, J. R. Williams, D. G. Ouellette, A. P. Kajdos, D. Goldhaber-Gordon, S. J. Allen and S. Stemmer, *Phys. Rev. X*, 2012, **2**, 021014.

26 F. Gunkel, K. Skaja, A. Shkabko, R. Dittmann, S. Hoffmann-Eifert and R. Waser, *Appl. Phys. Lett.*, 2013, **102**, 071601.

27 K. Zou, S. Ismail-Beigi, K. Kisslinger, X. Shen, D. Su, F. Walker and C. Ahn, *APL Mater.*, 2015, **3**, 036104.

28 Y. Chen, F. Trier, T. Kasama, D. V. Christensen, N. Bovet, Z. I. Balogh, H. Li, K. T. S. Thyden, W. Zhang, S. Yazdi, P. Norby, N. Pryds and S. Linderoth, *Nano Lett.*, 2015, **15**, 1849–1854.

29 J. Cheng, S. Nazir and K. Yang, *ACS Appl. Mater. Interfaces*, 2016, **8**, 31959–31967.

30 M. Dawber, C. Lichtensteiger, M. Cantoni, M. Veithen, P. Ghosez, K. Johnston, K. M. Rabe and J. M. Triscone, *Phys. Rev. Lett.*, 2005, **95**, 177601.

31 K. D. Fredrickson and A. A. Demkov, *Phys. Rev. B*, 2015, **91**, 115126.

32 G. Kresse and J. Furthmüller, *Comput. Mater. Sci.*, 1996, **6**, 15–50.

33 G. Kresse and J. Furthmüller, *Phys. Rev. B*, 1996, **54**, 11169–11186.

34 G. Kresse and D. Joubert, *Phys. Rev. B*, 1999, **59**, 1758–1775.

35 J. P. Perdew, K. Burke and M. Ernzerhof, *Phys. Rev. Lett.*, 1996, **77**, 3865–3868.

36 J. Sun, A. Ruzsinszky and J. P. Perdew, *Phys. Rev. Lett.*, 2015, **115**, 036402.

37 J. Heyd, G. E. Scuseria and M. Ernzerhof, *J. Chem. Phys.*, 2003, **118**, 8207–8215.

38 S. Curtarolo, G. L. W. Hart, M. B. Nardelli, N. Mingo, S. Sanvito and O. Levy, *Nat. Mater.*, 2013, **12**, 191–201.

39 R. Armiento, B. Kozinsky, M. Fornari and G. Ceder, *Phys. Rev. B*, 2011, **84**, 014103.

40 R. Guo, L. E. Cross, S.-E. Park, B. Noheda, D. E. Cox and G. Shirane, *Phys. Rev. Lett.*, 2000, **84**, 5423–5426.

41 M. Ghita, M. Fornari, D. J. Singh and S. V. Halilov, *Phys. Rev. B*, 2005, **72**, 054114.

42 X. Wu, S. Qin, T.-T. Gu, J. Yang and G. Manthilake, *Phys. Earth Planet. Inter.*, 2011, **189**, 151–156.

43 O. Müller and R. Roy, *The major ternary structural families*, Springer-Verlag, 1974.

44 R. A. Evarestov, *Phys. Rev. B*, 2011, **83**, 014105.

45 R. G. Burkovsky, D. Andronikova, Y. Bronwald, M. Krisch, K. Roleder, A. Majchrowski, A. V. Filimonov, A. I. Rudskoy and S. B. Vakhrushev, *J. Phys.: Condens. Matter*, 2015, **27**, 335901.

46 O. I. Prokopalo, I. P. Raevskii, M. A. Malitskaya, Y. M. Popov, A. A. Bokov and V. G. Smotrakov, *Ferroelectrics*, 1982, **45**, 89–95.

47 C. Rossel, M. Sousa, C. Marchiori, J. Fompeyrine, D. Webb, D. Caimi, B. Mereu, A. Ispas, J. Locquet, H. Siegwart, R. Germann, A. Tapponnier and K. Babich, *Microelec. Eng.*, 2007, **84**, 1869–1873.

48 H. Akamatsu, K. Fujita, H. Hayashi, T. Kawamoto, Y. Kumagai, Y. Zong, K. Iwata, F. Oba, I. Tanaka and K. Tanaka, *Inorg. Chem.*, 2012, **51**, 4560–4567.

49 A. Feteira, D. C. Sinclair, K. Z. Rajab and M. T. Lanagan, *J. Am. Ceram. Soc.*, 2008, **91**, 893–901.

50 E. Rauwel, A. Galeckas, P. Rauwel and H. Fjellvåg, *Adv. Fun. Mater.*, 2012, **22**, 1174–1179.

51 L.-G. Liu and A. Ringwood, *Earth Planet. Sci. Lett.*, 1975, **28**, 209–211.

52 H. Mizoguchi, H. W. Eng and P. M. Woodward, *Inorg. Chem.*, 2004, **43**, 1667–1680.

53 F. Sugawara, Y. Syono and S. Akimoto, *Mater. Res. Bull.*, 1968, **3**, 529–532.

54 G. Rohrer, *Structure and Bonding in Crystalline Materials*, Cambridge University Press, 2001.

55 S. H. Wemple, *Phys. Rev. B*, 1970, **2**, 2679–2689.

56 Y. Kuroiwa, S. Aoyagi, A. Sawada, J. Harada, E. Nishibori, M. Takata and M. Sakata, *Phys. Rev. Lett.*, 2001, **87**, 217601.

57 C. H. Peng, J.-F. Chang and S. B. Desu, *MRS Proceedings*, 1991, **243**, 21.

58 A. Krause, W. M. Weber, D. Pohl, B. Rellinghaus, A. Kersch and T. Mikolajick, *J. Phys. D: Appl. Phys.*, 2015, **48**, 415304.

59 L. S. Cavalcante, V. M. Longo, M. Zampieri, J. W. M. Espinosa, P. S. Pizani, J. R. Sambrano, J. A. Varela, E. Longo, M. L. Simões and C. A. Paskocimas, *J. Appl. Phys.*, 2008, **103**, 063527.

60 J. Kwapulinski, J. Kusz, H. BÃűhm and J. Dec, *J. Phys.: Condens. Matter*, 2001, **13**, 1461.

61 B. J. Kennedy, C. J. Howard and B. C. Chakoumakos, *Phys. Rev. B*, 1999, **59**, 4023–4027.

62 Y. S. Lee, J. S. Lee, T. W. Noh, D. Y. Byun, K. S. Yoo, K. Yamaura and E. Takayama-Muromachi, *Phys. Rev. B*, 2003, **67**, 113101.

63 I. D. Brown, *Chem. Soc. Rev.*, 1978, **7**, 359–376.

64 N. A. Benedek and C. J. Fennie, *J. Phys. Chem. C*, 2013, **117**, 13339–13349.

65 W. Setyawan, R. M. Gaume, S. Lam, R. S. Feigelson and S. Curtarolo, *ACS Comb. Sci.*, 2011, **13**, 382–390.

66 H. Sim, S. W. Cheong and B. G. Kim, *Phys. Rev. B*, 2013, **88**, 014101.

67 A. I. Lebedev, *Phys. of Solid State*, 2009, **51**, 362–372.

68 J. Kim, Y. Kim, Y. S. Kim, J. Lee, L. Kim and D. Jung, *Appl. Phys. Lett.*, 2002, **80**, 3581–3583.

69 K. Shibuya, T. Ohnishi, M. Lippmaa, M. Kawasaki and H. Koinuma, *Appl. Phys. Lett.*, 2004, **85**, 425–427.

70 S. A. Chambers, T. C. Kaspar, A. Prakash, G. Haugstad and B. Jalan, *Appl. Phys. Lett.*, 2016, **108**, 152104.

71 J. Cheng, J. Luo and K. Yang, *ACS Appl. Mater. Interfaces*, 2017, **9**, 7682–7690.

72 Y. Wang, W. Tang, J. Cheng, S. Nazir and K. Yang, *Phys. Chem. Chem. Phys.*, 2016, **18**, 31924–31929.

73 B. Yin and S. Qu, *Phys. Rev. B*, 2014, **89**, 014106.

74 X. Liu, Y. Wang, P. V. Lukashev, J. D. Burton and E. Y. Tsymbal, *Phys. Rev. B*, 2012, **85**, 125407.

75 Y. Liu, X. Lou, M. Bibes and B. Dkhil, *Phys. Rev. B*, 2013, **88**, 024106.

76 H. Lee, N. Campbell, J. Lee, T. J. Asel, T. R. Paudel, H. Zhou, J. W. Lee, B. Noesges, J. Seo, B. Park, L. J. Brillson, S. H. Oh, E. Y. Tsymbal, M. S. Rzchowski and C. B. Eom, *Nat. Mater.*, 2018, **17**, 231.

77 Y. Chen and N. Pryds, *Nat. Mater.*, 2018, **17**, 215.

78 Q. Yang, J. X. Cao, Y. Ma, Y. C. Zhou, X. J. Lou and J. Yang, *J. Appl. Phys.*, 2013, **114**, 034109.

79 R. M. Pick, M. H. Cohen and R. M. Martin, *Phys. Rev. B*, 1970, **1**, 910–920.

80 W. Zhong, R. D. King-Smith and D. Vanderbilt, *Phys. Rev. Lett.*, 1994, **72**, 3618–3621.

Table of Contents

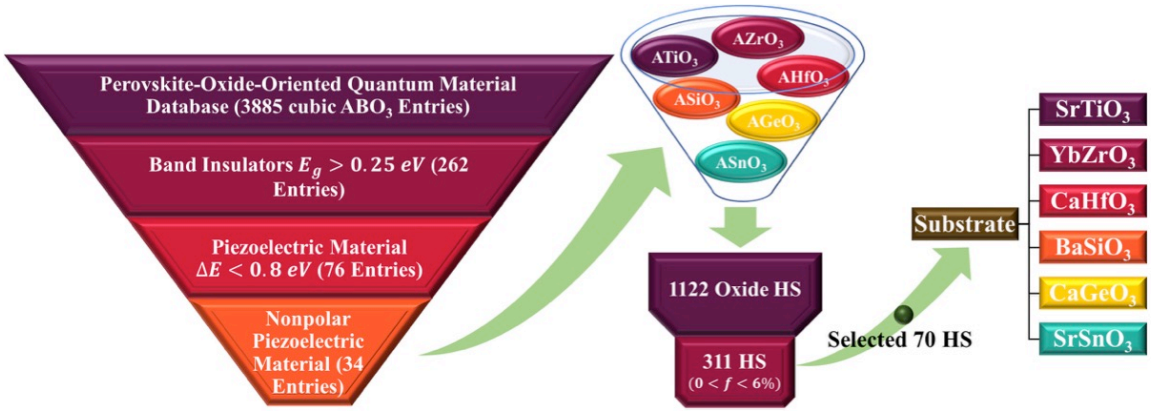

This work demonstrates an efficient approach to design perovskite-oxide-based two-dimensional electron gas using large-scale first-principles calculations.